Available online at www.sciencedirect.com
ScienceDirect
Journal of Sound and Vibration 300 (2007) 589–611
JOURNAL OF SOUND AND VIBRATION
www.elsevier.com/locate/jsvi

Modelling the vibration of sandwich beams using frequency-dependent parameters

D. Backström*, A.C. Nilsson

The Marcus Wallenberg Laboratory for Sound and Vibration Research, Department of Aeronautical and Vehicle Engineering, Kungl. Tekniska Högskolan, SE-100 44 Stockholm, Sweden

Received 27 May 2005; received in revised form 27 June 2006; accepted 5 July 2006
Available online 17 October 2006

Abstract

Various types of sandwich beams with foam or honeycomb cores are currently used in the industry, indicating the need for simple methods describing the dynamics of these complex structures. By implementing frequency-dependent parameters, the vibration of sandwich composite beams can be approximated using simple fourth-order beam theory. A higher-order sandwich beam model is utilized in order to obtain estimates of the frequency-dependent bending stiffness and shear modulus of the equivalent Bernoulli–Euler and Timoshenko models. The resulting predicted eigenfrequencies and transfer accellerance functions are compared to the data obtained from the higher-order model and from measurements.

1. Introduction

The type of sandwich structures considered in this article consist of two thin but relatively stiff sheets bonded to each side of a thick and light-weight core, see Fig. 1. A typical setup could be two aluminum sheets glued to a foam core, or— present in for example ship-building—steel plates bonded to a plastic core. Examples of widely used laminate materials are *glass-reinforced plastic*, abbreviated GRP, and carbon fiber. The purpose of the core is to maintain the distance between the laminates and to resist shear deformation, thus ideally maintaining pure bending of the beam around the neutral axis. This achieves the sought-for high static bending stiffness. Typical core configurations include plastic or metal foams and honeycomb materials. A different category of "sandwich" materials comprise plates consisting of two laminates separated by a visco-elastic layer designed to increase damping. The visco-elastic core layer deforms in shear parallell to the beam, i.e. in-plane deformation, whereas for the type of thick-core sandwich beams considered in this paper the principal shear deformation is in the lateral direction. This type of shear deformation was considered by Timoshenko in his derivation of thick-beam theory, see Refs. [1–3]. Constrained layer sandwich beams have been analyzed extensively for example in Refs. [4,5].

The dynamic response of a sandwich beam differs from that of an ordinary fourth-order beam in the high-frequency region. This is due to the more complex constitution of the structure, being a coupled system of two

*Corresponding author.
E-mail addresses: baxtrom@kth.se (D. Backström), achn@kth.se (A.C. Nilsson).

0022-460X/$ - see front matter © 2006 Elsevier Ltd. All rights reserved.
doi:10.1016/j.jsv.2006.07.048

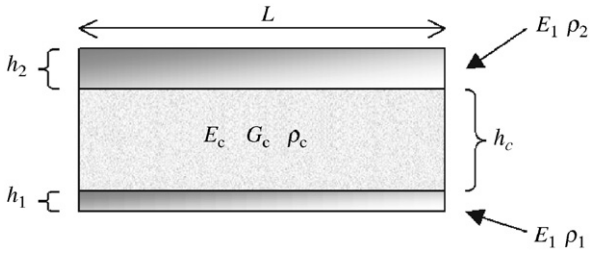

Fig. 1. An asymmetric sandwich beam.

thin beams and a thick core. The ordinary Bernoulli–Euler beam model neglects shear and rotational inertia and can be shown to rapidly deviate from the real dynamics of a sandwich. More refined theories taking these effects into account were presented by Lord Rayleigh and Timoshenko in Refs. [6,1], respectively. However, neither of these models is suitable for describing transverse vibration of composite beams. Bernoulli–Euler theory fails rapidly due to the assumption of an infinite shear modulus, and also Timoshenko theory fails since the vibration of a sandwich beam will be governed by the bending dynamics of the laminates at high frequencies; in terms of propagating waves, Timoshenko theory predicts that for high frequencies the deformation of the beam will be governed by the effects of shear and rotation, while for a three-layer sandwich beam with thin laminates and a soft core the high-frequency region is governed by pure bending of the laminates. Modelling the dynamics of layered beams and plates can be achieved in three different ways:

- Using exact formulation for the core deformation and solving the governing equations by means of numerical analysis.
- Imposing assumptions on the internal stress and deformation fields and thus obtaining finite-order equations which can be solved analytically.
- By utilizing models developed for homogenous beams and plates, in combination with effective or apparent parameters.

The first approach has been analyzed for example in Refs. [7,8] and compared to "elementary" methods in Ref. [9]. It is concluded that for most applications in the industry, finite-order models yield satisfactory solutions which make them attractive considering the increase of computational cost associated with "exact" models utilizing the general wave equation. The last item will be explored in this article and represents the simplest way of obtaining estimates for the various dynamic properties of layered beams and plates, such as vibration response, sound transmission loss and radiation.

Historically, research focusing on the flexural dynamics of composite beams and plates gained momentum after the war, when sandwich structures became an important part of aircraft construction:

- Kerwin [4] analyzed the damping of flexural waves in composites with viscoelastic layers.
- Mead and Markus [5] presented a sixth-order (bi-cubic) theory neglecting rotational inertia. In their paper, they investigated the response of a sandwich beam subject to "damped normal loadings" and presented orthogonality relations for the displacement of the beam.
- Rao and Nakra [10] analyzed the vibration of unsymmetrical sandwich beams with special attention to the effects of inertia.
- Mead [11] made a short review of different theories and also presented a model taking into account the effects of inertia and shear deformation in the laminates. Sixth- and eighth-order (bi-cubic and bi-quartic) equations of motion for symmetric and asymmetric sandwich beams were presented. However, no boundary conditions or exciting force distributions were imposed.
- Nilsson [7] presented an "exact" field equations model of a sandwich with thin laminates. The properties of this model were extensively investigated in Ref. [8], using laborious numerical methods to solve ill-conditioned sets of equations.

- Nilsson and Nilsson [12] instead suggested a sixth-order (bi-cubic) model derived using Hamilton's principle which describes the dynamics of a symmetric sandwich beam for frequencies below the mass–spring–mass frequency where the laminates start to move independently. This model was shown to yield accurate results when compared to measured data.

In the following section, a sixth-order sandwich beam theory for asymmetric beams is derived. This model will provide the basis for the development of modified lower-order models. The purpose of these simpler models is to provide means of analyzing the vibration of sandwich composite structures using existing tools developed for ordinary beams, for example formulae for the estimation of the sound transmission loss or vibration level of a sandwich panel. See Ref. [13] for a more detailed presentation, including the derivation of the tenth-order model mentioned briefly in Section 2.4.

2. High-order theory

The model presented in Refs. [14,12] is generalized to cover asymmetric sandwich structures, i.e. when the laminates are not equal. The governing set of equations are derived by applying Hamilton's principle, expressed as

$$\delta \int_{t_0}^{t_1} \int_0^L (U - T + A)\,\mathrm{d}x\,\mathrm{d}t = 0, \tag{1}$$

where δ here denotes the variation operator, U is the potential energy per unit length of the beam, T the kinetic energy per unit length and A the potential energy due to external forces (boundary conditions and applied forces and bending moments) per unit length. The spatial integration is over the length L of the beam, and the time integration limits t_0 and t_1 are arbitrary for an assumed stationary harmonic time dependence.

The total deformation w depends on x only since the core is assumed to be laterally incompressible, thus forcing the laminates to move in phase. This is a valid assumption well below the cut-on frequency for antiphase motion of the laminates, see Section 2.4. The geometric relation between w, the angle of pure bending β and the angle of pure shear γ is now given by

$$\frac{\partial w}{\partial x} = \beta + \gamma, \tag{2}$$

see Fig. 2.

The potential energy density U consists of three parts; energy due to pure bending β of the entire beam, shear in the core γ and pure bending of the thin laminates due to the shear deformation of the core. Thus, we have

$$U_1 = \frac{1}{2} D_{\mathrm{tot}} \left(\frac{\partial \beta}{\partial x}\right)^2,$$

$$U_2 = \frac{1}{2}(D_1 + D_2)\left(\frac{\partial \gamma}{\partial x}\right)^2, \tag{3}$$

$$U_3 = \tfrac{1}{2} G_c h_c \gamma^2,$$

where D_{tot} is the total bending stiffness per unit width of the sandwich beam, D_1 and D_2 are the bending stiffnesses of the laminates, and G_c is the effective core shear modulus. The total bending stiffness D_{tot} can be written as a weighted sum of the elasticity moduli of the laminates and the core,

$$D_{\mathrm{tot}} = c_0 E_1 + c_1 E_2 + c_2 E_c, \tag{4}$$

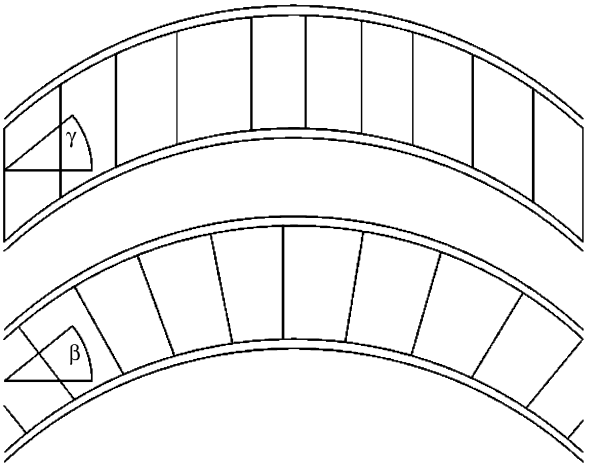

Fig. 2. Deformation mechanisms; γ due to pure shear of the core and β due to pure bending of the entire beam section.

where the c coefficients are given by

$$
\begin{aligned}
c_0 &= -y_0 h_1^2 + y_0^2 h_1 + \tfrac{1}{3} h_1^3, \\
c_1 &= \tfrac{1}{3}((h_1 + h_c + h_2)^3 - (h_1 + h_c)^3) + y_0^2 h_2 - y_0((h_1 + h_c + h_2)^2 - (h_1 + h_c)^2), \\
c_2 &= -y_0((h_1 + h_c)^2 - h_1^2) + y_0^2 h_c + \tfrac{1}{3}((h_1 + h_c)^3 - h_1^3),
\end{aligned}
$$

and the neutral layer coordinate y_0 is

$$
y_0 = \frac{h_1^2 E_1 + (2h_1 + h_c) E_c h_c + (2h_1 + 2h_c + h_2) E_2 h_2}{2(E_1 h_1 + E_c h_c + E_2 h_2)}.
$$

The bending stiffnesses per unit width of the laminates are

$$
D_i = \frac{E_i h_i^3}{12} \quad \text{for } i = 1, 2. \tag{5}
$$

The total kinetic energy density T is due to the velocity distribution $\dot{w}$ of the beam, and the angular velocity $\dot{\beta}$ of the sandwich cross-section:

$$
T_1 = \frac{1}{2} \mu_{\text{tot}} \left(\frac{\partial w}{\partial t} \right)^2,
$$

$$
T_2 = \frac{1}{2} I_{\text{tot}} \left(\frac{\partial \beta}{\partial t} \right)^2, \tag{6}
$$

where μ_{tot} is the total mass per unit area of the beam, and I_{tot} is the mass moment of inertia per unit width of the cross-section.

Finally, the boundary conditions and applied forces are accounted for in A as

$$
\int_0^L A \, \mathrm{d}x = -\int_0^L p(x) w(x) \, \mathrm{d}x - [Fw - M\beta - M_s \gamma]_0^L, \tag{7}
$$

where $p(x)$ is an external pressure exciting the beam, F is the shear force, M is the total bending moment and M_s is the bending moment acting on the laminates due to shear deformation in the core, all per unit width.

2.1. Governing equations

By performing the variation in Eq. (1), the governing equations are obtained

$$(D_1 + D_2)\left(\frac{\partial^4 w}{\partial x^4} - \frac{\partial^3 \beta}{\partial x^3}\right) - G_c h_c \left(\frac{\partial^2 w}{\partial x^2} - \frac{\partial \beta}{\partial x}\right) + \mu_{\text{tot}} \frac{\partial^2 w}{\partial t^2} - p = 0, \tag{8}$$

$$-D_{\text{tot}} \frac{\partial^2 \beta}{\partial x^2} + (D_1 + D_2)\left(\frac{\partial^3 w}{\partial x^3} - \frac{\partial^2 \beta}{\partial x^2}\right) - G_c h_c \left(\frac{\partial w}{\partial x} - \beta\right) + I_{\text{tot}} \frac{\partial^2 \beta}{\partial t^2} = 0, \tag{9}$$

with boundary conditions

$$F = -D_{\text{tot}} \frac{\partial^2 \beta}{\partial x^2} + I_{\text{tot}} \frac{\partial^2 \beta}{\partial t^2} \quad \text{or } w = 0, \tag{10}$$

$$M = -D_{\text{tot}} \frac{\partial \beta}{\partial x} \quad \text{or } \beta = 0, \tag{11}$$

$$M_s = -(D_1 + D_2)\left(\frac{\partial^2 w}{\partial x^2} - \frac{\partial \beta}{\partial x}\right) \quad \text{or } \frac{\partial w}{\partial x} = 0. \tag{12}$$

It can be verified that the above shear force and total bending moment satisfy basic equilibrium equations. Now, by assuming a time and space dependence of $e^{i(\omega t - kx)}$, where ω is the angular frequency and k the wavenumber for flexural waves, and combining Eqs. (8) and (9) with $p = 0$, the characteristic equation—or *dispersion relation*—gives the relationship between the wavenumber k and the frequency ω as

$$\begin{aligned}&(D_1 + D_2)D_{\text{tot}}k^6 + (G_c h_c D_{\text{tot}} - \omega^2 I_{\text{tot}}(D_1 + D_2))k^4 \\ &\quad - \omega^2(\mu_{\text{tot}}(D_1 + D_2 + D_{\text{tot}}) + G_c h_c I_{\text{tot}})k^2 + \mu_{\text{tot}}\omega^2(\omega^2 I_{\text{tot}} - G_c h_c) = 0.\end{aligned} \tag{13}$$

This is a sixth-order (bi-cubic) polynomial equation of even powers of k, and can be transformed into a third-order equation using a simple substitution. The magnitudes of the wavenumbers of a typical sandwich beam are shown in Fig. 3.

The solid curve represents the main propagating mode, whereas the dashed curve represents a nearfield below the cut-on frequency for rotational waves. The dotted curve represents a pure nearfield. The solutions to the dispersion relation are denoted $k = \pm\kappa_1$, $\pm i\kappa_2$ and $\pm i\kappa_3$. The κ quantities are real below the cut-on frequency for rotational waves, for systems without losses. This frequency, denoted by ω_{rot}, is obtained by

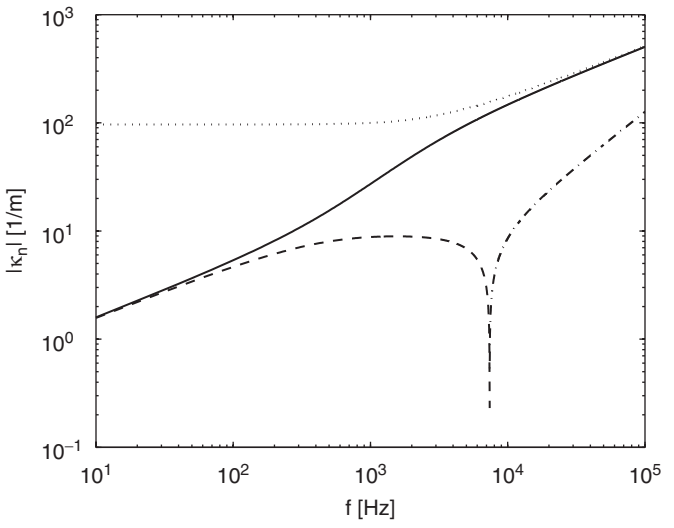

Fig. 3. Wavenumber magnitudes. —, κ_1, propagating; - -, κ_2, evanescent; - ·, κ_2, propagating; ···, κ_3, evanescent.

setting $k = 0$ in the dispersion relation. This yields

$$\omega_{\text{rot}} = \sqrt{\frac{G_c h_c}{I_{\text{tot}}}}. \tag{14}$$

The displacement and shear solutions are now given as

$$w(x,t) = \mathrm{e}^{\mathrm{i}\omega t}\sum_{n=1}^{6}\hat{A}_n \mathrm{e}^{-\mathrm{i}k_n x}, \quad \beta(x,t) = \mathrm{e}^{\mathrm{i}\omega t}\sum_{n=1}^{6}\hat{B}_n \mathrm{e}^{-\mathrm{i}k_n x},$$

or, using a different notation, as

$$w(x,t) = \{A_1\sin\kappa_1 x + A_2\cos\kappa_1 x + A_3\mathrm{e}^{-\kappa_2 x} + A_4\mathrm{e}^{\kappa_2(x-L)} + A_5\mathrm{e}^{-\kappa_3 x} + A_6\mathrm{e}^{\kappa_3(x-L)}\}\mathrm{e}^{\mathrm{i}\omega t}, \tag{15}$$

$$\beta(x,t) = \{B_1\sin\kappa_1 x + B_2\cos\kappa_1 x + B_3\mathrm{e}^{-\kappa_2 x} + B_4\mathrm{e}^{\kappa_2(x-L)} + B_5\mathrm{e}^{-\kappa_3 x} + B_6\mathrm{e}^{\kappa_3(x-L)}\}\mathrm{e}^{\mathrm{i}\omega t}. \tag{16}$$

The spatial dependences of Eqs. (15) and (16) are real for loss-free systems for frequencies below ω_{rot}. Inserting the above solutions into Eq. (9) and equating all coefficients of x-depending functions to zero yields a relationship between the A and B coefficients (or the corresponding $\hat{A}$ and $\hat{B}$ coefficients), reducing the problem to 6 unknowns, for example A_n. A good reason for preferring Eqs. (15) and (16) is that they are numerically more favorable.

2.2. Boundary conditions and mode shapes

The boundary conditions are given by Eqs. (10)–(12). Written in vector notation, where $\bar{\mathbf{A}}$ and $\bar{\mathbf{B}}$ contain the unknown coefficients, we have

$$\mathbf{Z}_1\bar{\mathbf{A}} + \mathbf{Z}_2\bar{\mathbf{B}} = \bar{\mathbf{0}}, \tag{17}$$

where the $\mathbf{Z}_1$ and $\mathbf{Z}_2$ matrices depend on the boundary conditions. The first three rows in $\mathbf{Z}_1$ and $\mathbf{Z}_2$ can be chosen to contain the boundary conditions for $x = 0$, and the last three rows the conditions for $x = L$. Further,

$$\bar{\mathbf{B}} = \mathbf{X}\bar{\mathbf{A}}, \tag{18}$$

where the matrix $\mathbf{X}$ is obtained by substituting Eqs. (15) and (16) into Eq. (9) and equating all coefficients of x-dependent functions to zero. Thus, for free vibration, the non-trivial solutions are given by the frequency condition

$$\det(\mathbf{Z}_1 + \mathbf{Z}_2\mathbf{X}) = 0, \tag{19}$$

and the corresponding null space vector. As an example, consider the case of *clamped* boundary conditions. From Eq. (10) we know that $w = 0$ at both ends, so the first row in $\mathbf{Z}_1$ will be given by the values of each subfunction in Eq. (15) for the displacement—i.e. $\sin(\kappa_1 x)$, $\cos(\kappa_1 x)$, $\mathrm{e}^{-\kappa_2 x}$ …—evaluated at $x = 0$. Similarly, the fourth row would contain the corresponding values evaluated at $x = L$. The second and fifth rows of $\mathbf{Z}_2$ are connected to Eq. (11). In this case, we have $\beta = 0$ at $x = 0$ and L. The final condition is given by Eq. (12) as $\partial w/\partial x = 0$, which occupies the third and sixth rows of $\mathbf{Z}_1$. Hence, with the rest of the elements being equal to zero, we have

$$\mathbf{Z}_1 = \begin{pmatrix} 0 & 1 & 1 & \mathrm{e}^{-\kappa_2 L} & 1 & \mathrm{e}^{-\kappa_3 L} \\ 0 & 0 & 0 & 0 & 0 & 0 \\ \kappa_1 & 0 & -\kappa_2 & \kappa_2\mathrm{e}^{-\kappa_2 L} & -\kappa_3 & \kappa_3\mathrm{e}^{-\kappa_3 L} \\ \sin(\kappa_1 L) & \cos(\kappa_1 L) & \mathrm{e}^{-\kappa_2 L} & 1 & \mathrm{e}^{-\kappa_3 L} & 1 \\ 0 & 0 & 0 & 0 & 0 & 0 \\ \kappa_1\cos(\kappa_1 L) & -\kappa_1\sin(\kappa_1 L) & -\kappa_2\mathrm{e}^{-\kappa_2 L} & \kappa_2 & -\kappa_3\mathrm{e}^{-\kappa 3L} & \kappa_3 \end{pmatrix},$$

and

$$\mathbf{Z}_2 = \begin{pmatrix} 0 & 0 & 0 & 0 & 0 & 0 \\ 0 & 1 & 1 & e^{-\kappa_2 L} & 1 & e^{-\kappa_3 L} \\ 0 & 0 & 0 & 0 & 0 & 0 \\ 0 & 0 & 0 & 0 & 0 & 0 \\ \sin(\kappa_1 L) & \cos(\kappa_1 L) & e^{-\kappa_2 L} & 1 & e^{-\kappa_3 L} & 1 \\ 0 & 0 & 0 & 0 & 0 & 0 \end{pmatrix}.$$

The sought-for relationship between the A and B coefficients, yielding the $\mathbf{X}$ matrix, is obtained as

$$B_1 = X_2 A_2, \quad B_2 = X_1 A_1, \quad B_3 = X_3 A_3,$$

$$B_4 = X_4 A_4, \quad B_5 = X_5 A_5, \quad B_6 = X_6 A_6, \tag{20}$$

where

$$X_1 = -X_2 = \frac{\kappa_1\{(D_1 + D_2)\kappa_1^2 + G_c h_c\}}{(D_{\text{tot}} + D_1 + D_2)\kappa_1^2 + G_c h_c - \omega^2 I_{\text{tot}}},$$
$$X_3 = -X_4 = -\frac{\kappa_2\{(D_1 + D_2)\kappa_2^2 + G_c h_c\}}{(D_{\text{tot}} + D_1 + D_2)\kappa_2^2 + G_c h_c - \omega^2 I_{\text{tot}}},$$
$$X_5 = -X_6 = -\frac{\kappa_3\{(D_1 + D_2)\kappa_3^2 + G_c h_c\}}{(D_{\text{tot}} + D_1 + D_2)\kappa_3^2 + G_c h_c - \omega^2 I_{\text{tot}}}.$$

Now, by computing the roots of Eq. (19)—using some numerical method like the *secant method* or *Newton's method*—the eigenfrequencies ω_m of the sandwich configuration are obtained.

For *simply supported* boundary conditions, it can be seen directly from the corresponding system matrix $\mathbf{M} = \mathbf{Z}_1 + \mathbf{Z}_2\mathbf{X}$ that the eigenfrequencies will be given by inserting

$$kL = m\pi, \quad m \in \mathbb{N}$$

into the dispersion relation Eq. (13), yielding

$$\omega_m = \frac{m^2\pi^2}{L^2}\sqrt{\frac{D_{\text{tot}}\{(D_1 + D_2)\pi^2 m^2 + G_c h_c L^2\}}{\mu_{\text{tot}}\{(D_{\text{tot}} + D_1 + D_2)\pi^2 m^2 + G_c h_c L^2\}}}. \tag{21}$$

By comparing Eq. (21) with the well-known expression for the eigenfrequencies of simply supported Bernoulli–Euler beams,

$$\omega_m^{\text{BE}} = \frac{m^2\pi^2}{L^2}\sqrt{\frac{D}{\mu}}, \tag{22}$$

where D is the bending stiffness and μ is mass per unit area of the homogenous beam, one can readily identify a discrete estimate of the *apparent bending stiffness* D_{app} of the simply supported sandwich beam as

$$D_{\text{app}}^{(m)} = \frac{D_{\text{tot}}\{(D_1 + D_2)\pi^2 m^2 + G_c h_c L^2\}}{(D_{\text{tot}} + D_1 + D_2)\pi^2 m^2 + G_c h_c L^2}. \tag{23}$$

$D_{\text{app}}^{(m)}$ is the apparent value of the bending stiffness of an ordinary Bernoulli–Euler beam, with the same dimensions and mass, at the mth resonance. These modified lower-order beam models will be more carefully analyzed later in this article.

Calculating the mode shapes of a sandwich configuration involves solving the nullspace problem $\mathbf{M}\bar{\mathbf{A}} = \bar{\mathbf{0}}$, where $\mathbf{M} = \mathbf{Z}_1 + \mathbf{Z}_2\mathbf{X}$ is a known matrix. A simple way of doing this is to assume a unit first element of the $\bar{\mathbf{A}}$

vector, so that the system can be written

$$\begin{pmatrix} \alpha & \bar{\mathbf{W}}^{\mathrm{T}} \\ \bar{\mathbf{V}} & \mathbf{M}_{\mathrm{sub}} \end{pmatrix} \begin{pmatrix} 1 \\ \bar{\mathbf{A}}_{\mathrm{sub}} \end{pmatrix} = \bar{\mathbf{0}},$$

where α is a scalar, $\bar{\mathbf{V}}$ and $\bar{\mathbf{W}}$ are vectors, $\mathbf{M}_{\mathrm{sub}}$ a matrix and $\bar{\mathbf{A}}_{\mathrm{sub}}$ a vector. Now, by expanding, we obtain

$$\bar{\mathbf{V}} + \mathbf{M}_{\mathrm{sub}}\bar{\mathbf{A}}_{\mathrm{sub}} = \bar{\mathbf{0}}. \tag{24}$$

This system can be solved in order to obtain the unknown elements given by the $\bar{\mathbf{A}}_{\mathrm{sub}}$ elements, defining the $\bar{\mathbf{A}}$ and $\bar{\mathbf{B}}$ coefficients. Predicted normalized modeshapes for a clamped sandwich beam are shown in Fig. 4.

2.3. Forced response

The inhomogenous problem—when a force or bending moment distribution is exciting the beam—can be solved in terms of *Green's functions*. Consider a beam excited by a lateral point force per unit width $F_0 e^{i\omega t}$ at $x = x_0$, see Fig. 5.

Denote the deformation solutions for $0 < x < x_0$ by w_- and β_-, and the corresponding solutions for $x_0 < x < L$ by w_+ and β_+. For numerical reasons, it is preferable to use the following sets of base functions for

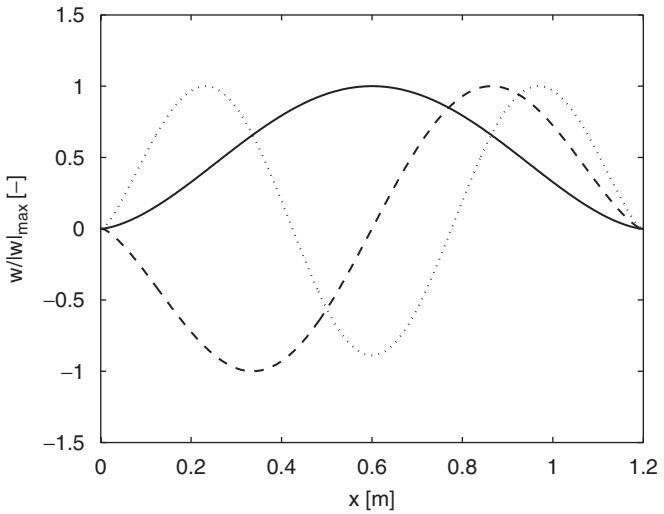

Fig. 4. Mode shapes, clamped conditions: —, mode 1; - -, mode 2; ···, mode 3.

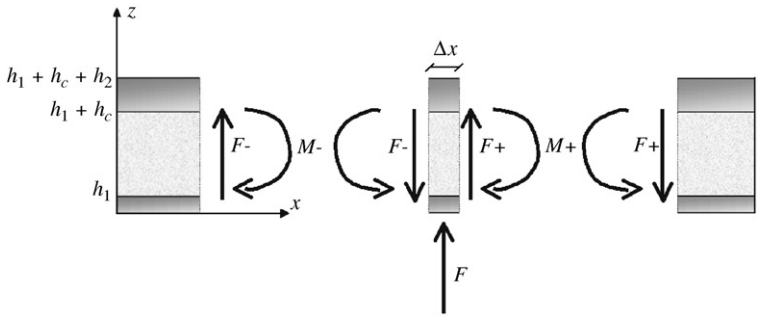

Fig. 5. A point force acting on a sandwich beam.

the solutions, as compared to that used in Eqs. (15) and (16)

$$\bar{\mathbf{b}}_- = (\sin\kappa_1 x, \cos\kappa_1 x, \mathrm{e}^{-\kappa_2 x}, \mathrm{e}^{\kappa_2(x-x_0)}, \mathrm{e}^{-\kappa_3 x}, \mathrm{e}^{\kappa_3(x-x_0)})^{\mathrm{T}},$$
$$\bar{\mathbf{b}}_+ = (\sin\kappa_1(L-x), \cos\kappa_1(L-x), \mathrm{e}^{-\kappa_2(L-x)}, \mathrm{e}^{\kappa_2(x_0-x)}, \mathrm{e}^{-\kappa_3(L-x)}, \mathrm{e}^{\kappa_3(x_0-x)})^{\mathrm{T}}. \tag{25}$$

We have to consider the fact that their respective $\mathbf{X}$ matrices are different; it is easy to see that in this particular case $\mathbf{X}_+ = -\mathbf{X}_- = -\mathbf{X}$. Now, the boundary conditions at $x = 0$ and $x = L$ together with the coupling conditions at $x = x_0$ yields a system of 12 equations, sufficient to solve for the unknown coefficient vectors $\bar{\mathbf{A}}_-$ and $\bar{\mathbf{A}}_+$ as functions of the exciting force amplitude F_0. In matrix notation, where $\mathbf{M}_-$ and $\mathbf{M}_+$ are the 3×6 boundary condition matrices at $x = 0$ and $x = L$, respectively,

$$\begin{pmatrix} \mathbf{M}_- & \mathbf{0} \\ & \mathbf{M}_c \\ \mathbf{0} & \mathbf{M}_+ \end{pmatrix} \begin{pmatrix} \bar{\mathbf{A}}_- \\ \bar{\mathbf{A}}_+ \end{pmatrix} = \bar{\mathbf{F}}, \tag{26}$$

where $\mathbf{M}_c$ is a 6×12 matrix describing the coupling conditions. $\bar{\mathbf{F}}$ contains the force amplitude F_0 as its only non-zero element. The coupling conditions are obtained from Eqs. (10) to (12), together with conditions regarding continuity in total deflection w, the total deflection angle $\partial w/\partial x$ and the bending angle β.

This leads to the six coupling conditions at $x = x_0$, defining $\mathbf{M}_c$ and $\bar{\mathbf{F}}$:

$$w_- = w_+, \tag{27}$$

$$\frac{\partial w_-}{\partial x} = \frac{\partial w_+}{\partial x}, \tag{28}$$

$$\beta_- = \beta_+, \tag{29}$$

$$\frac{\partial \beta_-}{\partial x} = \frac{\partial \beta_+}{\partial x}, \tag{30}$$

$$\frac{\partial^2 w_-}{\partial x^2} = \frac{\partial^2 w_+}{\partial x^2}, \tag{31}$$

$$(D_1 + D_2)\left(\frac{\partial^3 w_-}{\partial x^3} - \frac{\partial^2 \beta_-}{\partial x^2}\right) - G_c h_c\left(\frac{\partial w_-}{\partial x} - \beta_-\right)$$
$$- (D_1 + D_2)\left(\frac{\partial^3 w_+}{\partial x^3} - \frac{\partial^2 \beta_+}{\partial x^2}\right) + G_c h_c\left(\frac{\partial w_+}{\partial x} - \beta_+\right) = F_0. \tag{32}$$

Here, Eqs. (30) and (31) are obtained indirectly from combining Eqs. (11) and (12). Implementing the coupling conditions in this order implies that the ninth element of $\bar{\mathbf{F}}$ contains F_0, the other elements being equal to zero. The result is a governing 12×12 matrix system, which can be solved using some numerical software tool like Matlab, obtaining the displacement fields w, β and indirectly γ for any given point force exciting the beam

$$w(x,t) = \begin{cases} \mathrm{e}^{\mathrm{i}\omega t}\bar{\mathbf{A}}_-^{\mathrm{T}}\bar{\mathbf{b}}_-, & x \leqslant x_0 \\ \mathrm{e}^{\mathrm{i}\omega t}\bar{\mathbf{A}}_+^{\mathrm{T}}\bar{\mathbf{b}}_+, & x \geqslant x_0 \end{cases} \quad \beta(x,t) = \begin{cases} \mathrm{e}^{\mathrm{i}\omega t}\bar{\mathbf{B}}_-^{\mathrm{T}}\bar{\mathbf{b}}_-, & x \leqslant x_0, \\ \mathrm{e}^{\mathrm{i}\omega t}\bar{\mathbf{B}}_+^{\mathrm{T}}\bar{\mathbf{b}}_+, & x \geqslant x_0. \end{cases} \tag{33}$$

For more complex force distributions, the solution is given as an integral over the length of the beam

$$w(x,t) = \mathrm{e}^{\mathrm{i}\omega t}\int_0^L G_w(x,\chi)F'(\chi)\,\mathrm{d}\chi, \tag{34}$$

where $G_w(x,\chi)$ is the displacement at x corresponding to a unit point force applied at χ, obtained from Eq. (33), and $F'(\chi)$ is the force distribution (force per unit length and width) as a function of the position variable χ. Analogously, the bending angle field β can be obtained from the corresponding Green's function $G_\beta(x,\chi)$.

The case of simply supported end conditions can be treated separately by expressing the solutions for w and β in terms of sin and cos series expansions, respectively. This is due to the fact that these sets of functions

satisfy the boundary conditions as well as provide a full base for the solutions. Thus, considering point excitation, we let

$$w = \mathrm{e}^{\mathrm{i}\omega t}\sum_{n=1}^{\infty}\mathscr{A}_n\phi_n(x), \quad \beta = \mathrm{e}^{\mathrm{i}\omega t}\sum_{n=1}^{\infty}\mathscr{B}_n\psi_n(x), \tag{35}$$

where the orthogonal ϕ and ψ functions are given by

$$\phi_n(x) = \sin\frac{n\pi x}{L}, \quad \psi_n(x) = \cos\frac{n\pi x}{L}. \tag{36}$$

$\mathscr{A}_n$ and $\mathscr{B}_n$ are coefficient sets to be determined, and should not be confused with the A_n and B_n sets introduced earlier. It can be noted that since $n>0$, the cosine series expansion is incomplete. However, the $\mathscr{B}_0$ term corresponds to rigid body rotation and is of no interest.

Inserting these ansatzes into the governing Eqs. (8) and (9) yields, with time dependence excluded,

$$\sum_{n=1}^{\infty}\left\{\frac{n\pi}{L}\left(\frac{n^2\pi^2}{L^2}(D_1+D_2)+G_ch_c\right)\left(\frac{n\pi}{L}\mathscr{A}_n-\mathscr{B}_n\right)-\omega^2\mu_{\mathrm{tot}}\mathscr{A}_n\right\}\phi_n(x) = p(x), \tag{37}$$

$$\sum_{n=1}^{\infty}\left\{\frac{n^2\pi^2}{L^2}\left(D_{\mathrm{tot}}\mathscr{B}_n-(D_1+D_2)\left(\frac{n\pi}{L}\mathscr{A}_n-\mathscr{B}_n\right)\right)-G_ch_c\left(\frac{n\pi}{L}\mathscr{A}_n-\mathscr{B}_n\right)-\omega^2 I_{\mathrm{tot}}\mathscr{B}_n\right\}\psi_n(x) = 0. \tag{38}$$

By assuming a point excitation on the form $p(x) = F_0\delta(x-x_0)$, where F_0 is per unit width of the beam, and taking the inner products over the length of the beam of Eqs. (37) and (38) with $\phi_q(x)$ and $\psi_q(x)$, respectively, we obtain

$$\left\{\frac{n\pi}{L}\left(\frac{n^2\pi^2}{L^2}(D_1+D_2)+G_ch_c\right)\left(\frac{n\pi}{L}\mathscr{A}_n-\mathscr{B}_n\right)-\omega^2\mu_{\mathrm{tot}}\mathscr{A}_n\right\}\frac{L}{2} = F_0\phi_n(x_0), \tag{39}$$

$$\frac{n^2\pi^2}{L^2}\left(D_{\mathrm{tot}}\mathscr{B}_n-(D_1+D_2)\left(\frac{n\pi}{L}\mathscr{A}_n-\mathscr{B}_n\right)\right)-G_ch_c\left(\frac{n\pi}{L}\mathscr{A}_n-\mathscr{B}_n\right)-\omega^2 I_{\mathrm{tot}}\mathscr{B}_n = 0. \tag{40}$$

The result is a 2×2 algebraic system which yields the $\mathscr{A}_n$ and $\mathscr{B}_n$ coefficients as functions of the exciting force amplitude per unit width, F_0. Approximate mobility functions can be obtained numerically in terms of truncated mode sums. Note also that by calculating the determinant of the matrix system—i.e the denominator of each mode in the mode expansion—we obtain the ordinary frequency relationship of $\omega_n^2-\omega^2$, where ω_n is given by Eq. (21). The expression for the total displacement w can be shown to be identical to that of the ordinary Bernoulli–Euler theory, the only difference being the values of the eigenfrequencies ω_n:

$$w(x,t) = \frac{2F_0\mathrm{e}^{\mathrm{i}\omega t}}{L\mu_{\mathrm{tot}}}\sum_{n=1}^{\infty}\frac{\sin(n\pi x_0/L)\sin(n\pi x/L)}{\omega_n^2-\omega^2}. \tag{41}$$

2.4. Notes on a tenth-order model including the effects of core compressibility

The effects of core compressibility was included in a more advanced model, where the core deflection and shear deformation were described by linearly interpolating the deformations of the laminates. However, this tenth-order model turned out to be numerically cumbersome and therefore not of great interest. It could potentially become valuable for predicting the vibration of sandwich beams with heavy laminates and soft cores, where the *mass–spring–mass frequency* of the system, i.e the cut-on frequency for independent vibration of the laminates, is forced down into the considered frequency range. Another application could be for fluid-loaded plates.

2.5. Implementing losses

Losses can be easily implemented into the model by means of complex elasticity moduli, in accordance with common practice. Thus,

$$E_n = \mathrm{Re}(E_n)(1 + \mathrm{i}\eta_n), \quad n = 1, 2,$$
$$E_c = \mathrm{Re}(E_c)(1 + \mathrm{i}\eta_c), \tag{42}$$
$$G_c = \mathrm{Re}(G_c)(1 + \mathrm{i}\eta_c),$$

where E_n and η_n denote the elasticity moduli and loss factors of the laminates, respectively, and E_c, G_c and η_c the elasticity modulus, shear modulus and loss factor of the core.

3. Apparent bending stiffness

A different approach to modelling the flexural response of sandwich composites is provided by the concept of *apparent bending stiffness*. The idea is to implement a frequency-dependent bending stiffness parameter, denoted $D_{\mathrm{app}}(\omega)$, in the ordinary Bernoulli–Euler beam theory or the corresponding Kirchhoff plate theory. The frequency dependence of D_{app} is chosen such that the thin-beam theory as accurately as possible mimics the true response of the composite beam.

However, it should be stressed that apparent bending stiffness is an approximate tool. Naturally, it is impossible to correctly describe the combined effects of the propagating mode and the nearfields using only one wavenumber. The most intuitive way to deal with this problem is to assume that D_{app} depends on boundary conditions, while another option is to discard[1] the k_3 wavenumber and implement Timoshenko theory instead of Bernoulli–Euler theory. The latter possibility will be analyzed later.

It can also be mentioned that instead of implementing a single, frequency-dependent bending stiffness parameter $D_{\mathrm{app}}(\omega)$ to be shared by all modes, it is possible to assign a unique bending stiffness $D_{\mathrm{app}}^{(m)}$ to each mode, using for example Eq. (23) in the case of a simply supported sandwich beam. The advantage of this approach is that calculated mobilities will not suffer from "narrowing" of its peaks, which is otherwise the case when using a frequency-dependent smooth bending stiffness curve. See the discussions in Sections 3.3 and 6.

In summary, the apparent bending stiffness concept is an approximate engineering approach, "translating" a sandwich beam into an ordinary homogenous beam. Various ways of obtaining estimates of $D_{\mathrm{app}}(\omega)$ will be given in the following section.

3.1. Different estimates of D_{app}

3.1.1. Method of displacement error minimization

There are several possible estimates of the D_{app} parameter. One definition could require the minimization of the mean displacement error with respect to D_{app},

$$E(D_{\mathrm{app}}, \omega) = \frac{1}{L}\int_0^L |w - w_{\mathrm{app}}|\,\mathrm{d}x, \tag{43}$$

where w is the "true" deflection as calculated by Eq. (33) and w_{app} is the deflection yielded by applying Bernoulli–Euler theory with a frequency-dependent bending stiffness. However, this is a rather cumbersome approach as it involves the full solution to the sixth-order problem. Further, once the full solution is obtained, a numerical approach to solving the minimization problem is probably required if the absolute error definition is to be used. As an alternative, the least-squares method could be considered.

Besides from the computational disadvantages of this definition, another problem lies in the fact that the obtained estimate of D_{app} must depend on the chosen type of excitation force distribution. In Fig. 6, point

[1]In a wide frequency region, the magnitude of κ_3 is much larger than those of the other wavenumbers. This implies that the nearfield associated with κ_3 is highly localized to edges and discontinuities, and will not influence the displacement some distance away from these.

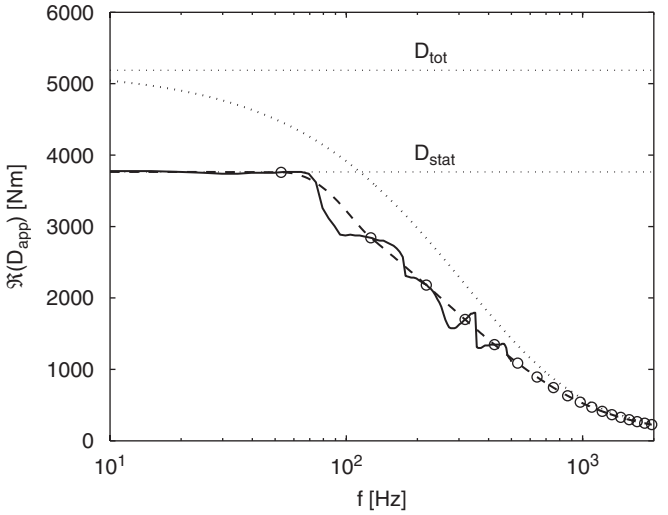

Fig. 6. Different estimates of D_{app} for the sample sandwich beam specified in Table 3, with both ends clamped. —, numerical error minimization; - -, method of equating eigenfrequencies; $\cdots$, κ_1-method; ○, eigenfrequencies.

excitation has been utilized. Also note that the chosen cost function could be replaced by for example kinetic energy error, yielding a different estimate.

3.1.2. κ_1-method

In contrast to the previous definition, the simplest estimate of D_{app} is obtained by inserting the main propagating wavenumber κ_1 into the Bernoulli–Euler dispersion relation, solving for the bending stiffness. This yields

$$D_{app} = \frac{\mu_{tot}\omega^2}{\kappa_1^4}. \tag{44}$$

The problem with this approach is the discarding of the two other wavenumbers, implying that the effects of nearfields are not described as accurately as they could be. As mentioned earlier, the apparent bending stiffness—as applicable to Bernoulli–Euler theory—should depend on boundary conditions, in order to achieve an accurate description of the problem. For example, using this approach one will obtain the same eigenfrequencies for both clamped and free end conditions. This is true for Bernoulli–Euler beams, but not for sandwich composites. Also, the low-frequency asymptote will in general be overestimated. This problem can be illustrated as follows: consider the maximum static deflection for a sandwich beam subject to a central point force F per unit width (obtained from thick beam statics, see for example Ref. [15]):

$$\delta_{max} = F\left(\frac{q_b L^3}{D_{tot}} + \frac{q_s L}{G_c h_c}\right). \tag{45}$$

Here, q_b and q_s are the *bending deflection coefficient* and *shear deflection coefficient*, respectively, and depend on boundary conditions (see Table 1). For an equivalent Bernoulli–Euler beam the corresponding expression is given by

$$\delta_{max}^{BE} = F\frac{q_b L^3}{D_{app}^{stat}}. \tag{46}$$

By equating the maximum deflections and solving for the static equivalent bending stiffness D_{app}^{stat}, we obtain

$$D_{app}^{stat} = \frac{D_{tot}}{1 + \dfrac{q_s D_{tot}}{q_b L^2 G_c h_c}}. \tag{47}$$

Table 1
Bending and shear coefficients for different boundary conditions, static deflection

	q_b^{-1}	q_s^{-1}
Simply supported (central load)	48	4
Clamped–clamped (central load)	192	4
Clamped–free (end load)	3	1

Table 2
Approximate values of $\kappa_m L$ for some simple boundary conditions

m	1	2	3	$\geqslant 4$
Simply supported	π	2π	3π	$m\pi$
Free–free or clamped–clamped	4.730	7.853	10.996	$\frac{2m+1}{2}\pi$
Clamped–simply supported	3.927	7.069	10.210	$\frac{4m+1}{4}\pi$
Clamped–free	1.875	4.694	7.855	$\frac{2m-1}{2}\pi$

It is clear that the apparent bending stiffness will converge to a value lower than D_{tot}, for finite values of the shear modulus and beam length.

3.1.3. Method of equating eigenfrequencies

The most intuitive approach to obtaining a boundary condition dependent estimate is to consider eigenfrequencies. These can be obtained in a relatively straight-forward way from the sixth-order method, see Eq. (19). The eigenfrequencies of a Bernoulli–Euler beam is given, for different boundary conditions, by

$$\omega_m^{\text{BE}} = \kappa_m^2 \sqrt{\frac{D}{\mu}}, \tag{48}$$

where κ_m[2]depends on boundary conditions, see Table 2.

Now, by calculating the eigenfrequencies ω_m of a given sandwich beam configuration, a discrete estimate of D_{app} can be obtained from Eq. (48) as

$$D_{\text{app}}^{(m)} = \begin{cases} D_{\text{app}}^{\text{stat}}, & m = 0, \\ \dfrac{\omega_m^2 \mu_{\text{tot}}}{\kappa_m^4}, & m > 0. \end{cases} \tag{49}$$

This is consistent with earlier results, see Eq. (23). In order to obtain a continuous estimate, some type of interpolation scheme can be used. In Fig. 6 piecewise cubic interpolation has been utilized.

In Fig. 7, the influence on the apparent bending stiffness of different boundary conditions is presented.

3.2. Apparent loss factor

By using complex valued elasticity and shear moduli the loss factors of the laminates and the core are implemented in the full model. For the Bernoulli–Euler model, however, a frequency-dependent total loss factor η_{app} must be used. An estimate for this entity can be obtained from the dispersion relation by using the complex-valued material parameters. It is intuitive to assume that the apparent loss factor is proportional to

[2]The eigenvalues κ_m, $m \in \mathbb{N}$, should not be confused with the continuous κ_1, κ_2 and κ_3 solutions to the sixth-order dispersion relation.

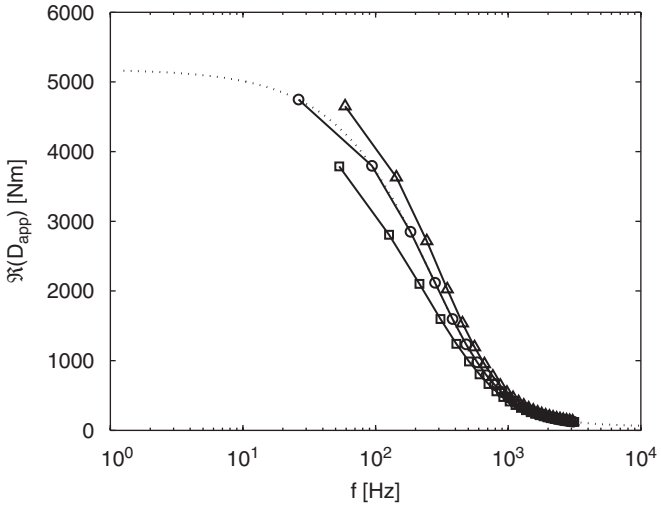

Fig. 7. Different values of the apparent bending stiffness of the sandwich beam specified in Table 3, depending on boundary conditions. ○, simply supported ends; □, clamped ends; △, free ends; ···, κ_1-method.

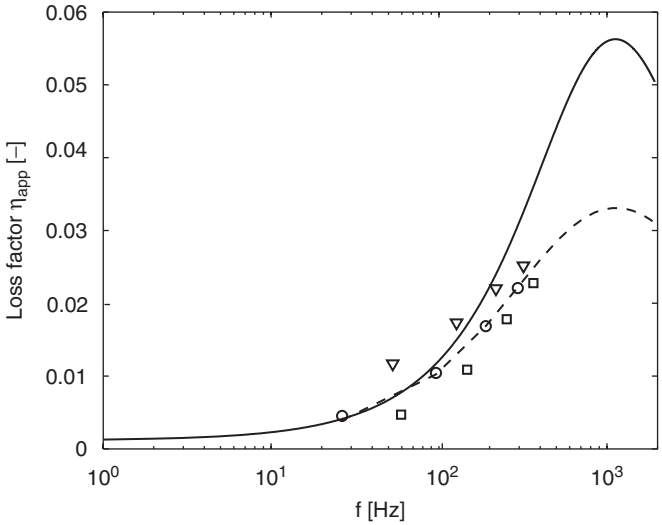

Fig. 8. Estimates of the apparent loss factor, using the *half-power bandwidth method*, which is described for example in Ref. [3]. The method was manually applied to accelerance graphs obtained from the sixth-order model. —, from κ_1; - -, from Eq. (23); ○, simply supported ends; □, free ends; ∇, clamped ends.

the imaginary part of the main wavenumber, as is done in Ref. [7], i.e.

$$\kappa_1 = \mathrm{Re}(\kappa_1)\left(1 - \frac{\mathrm{i}\eta_{\mathrm{app}}}{4}\right) \rightarrow \eta_{\mathrm{app}} = -4\frac{\mathrm{Im}(\kappa_1)}{\mathrm{Re}(\kappa_1)}. \tag{50}$$

The result is represented by the solid curve in Fig. 8.

Other possible ways of obtaining estimates of the apparent loss factor include analysis of measured or calculated transfer functions or reverberation time—the *half-power bandwidth method* was used to obtain estimates of the apparent loss factors for different boundary conditions, see Fig. 8. As could be expected, clamped end conditions seem to imply a higher apparent loss factor than the simply supported case, and free end conditions seem to imply a lower loss factor.

The dashed curve represents the loss factor estimate given by Eq. (23), as the ratio of the imaginary part to the real part. The prediction agrees well with the higher-order theory, for simply supported beams. As mentioned earlier, the denominator of each mode amplitude can be written as $\omega_n^2-\omega^2$, where ω_n is obtained from Eq. (21) or indirectly Eq. (23). Using complex material parameters, the imaginary part of ω_n^2 will be proportional to the effective loss factor η_{app}. Hence, it seems justified to use Eq. (23) with complex-valued material parameters to describe the forced motion of lightly damped, simply supported sandwich beams.

Losses can now be implemented in the simplified model by assuming a complex apparent bending stiffness $D_{\text{app}} = \text{Re}(D_{\text{app}})(1 + \text{i}\eta_{\text{app}})$. The loss factors of the aluminum laminates were assumed to be approximately equal to 10^{-3} while for the plastic foam core a value of 0.04 was used. The latter value was obtained by comparing the results of the full model to measured data.

3.3. Implementing the apparent bending stiffness

Obtaining transfer function and mode shape estimates using the sixth-order theory involves complicated numerical procedures. In contrast, the "equivalent" Bernoulli–Euler theory is simple to implement. For example, the deflection of a beam subject to some force distribution F' per unit length is given by [3]

$$w(x,t) = \text{e}^{\text{i}\omega t}\sum_{m=0}^{\infty}\frac{\langle F',\ \phi_m\rangle\phi_m}{b(D\kappa_m^4-\mu\omega^2)\langle\phi_m,\phi_m\rangle}, \tag{51}$$

where ϕ_m are the eigenfunctions and κ_m the eigenvalues corresponding to the particular boundary conditions, b is the width of the beam and $\langle\cdot,\cdot\rangle$ is the inner product operator. For a sandwich beam element, the bending stiffness D is replaced by the frequency-dependent $D_{\text{app}}(\omega)$ or the discrete $D_{\text{app}}^{(m)}$. The latter option is preferable in a mechanical viewpoint, since using a constant D_{app} for each mode implies a better description of the width of the resonance peaks. However, the frequency dependent estimate may be simpler to implement in various applications.

It should be noted that using a constant value of the bending stiffness for each mode is not the same thing as to let all modes share the same frequency-dependent bending stiffness. A close approximation to the mode-discrete case could be achieved by implementing a piecewise constant bending stiffness curve, where the bending stiffness is constant in a region around each eigenfrequency, allowing the width of the resonance peaks to be correctly described locally. This could be what the error-minimizing numerical algorithm is trying to show in Fig. 6. However, implementing a discontinuous bending stiffness would also imply discontinuous mobility curves, phase velocities and so on.

4. An equivalent Timoshenko beam approach

As stated in the previous section, the greatest disadvantage of the equivalent Bernoulli–Euler beam is the need for a boundary condition-dependent estimate of the apparent bending stiffness. By instead utilizing an equivalent Timoshenko beam, where the κ_3 wavenumber is discarded, it is possible to find frequency-dependent bending stiffness and shear modulus parameters such that the Timoshenko wavenumbers coincide with κ_1 and κ_2. This effectively means dividing the sixth-order sandwich dispersion relation by $k^2+\kappa_3^2$, which yields a reduced fourth-order dispersion polynomial. This approach assumes that the effects of the nearfields associated with κ_3 are negligible.

Consider a fourth-order polynomial of even powers in k, with roots equal to the wavenumbers $\pm\kappa_1$ and $\pm\text{i}\kappa_2$ of the sixth-order sandwich theory (see Fig. 3 for frequencies well below ω_{rot}):

$$(k-\kappa_1)(k+\kappa_1)(k-\text{i}\kappa_2)(k+\text{i}\kappa_2) = k^4+(\kappa_2^2-\kappa_1^2)k^2-\kappa_1^2\kappa_2^2. \tag{52}$$

This expression is compared to the dispersion relation of a Timoshenko beam, which is obtained from Eq. (13) by setting $D_1 = D_2 = 0$. Assuming the rotational inertia I_{tot} is negligible, we obtain

$$k^4-\frac{\mu_{\text{tot}}\omega^2}{G_{\text{app}}^{\text{T}}h_c}k^2-\frac{\mu_{\text{tot}}\omega^2}{D_{\text{app}}^{\text{T}}} = 0, \tag{53}$$

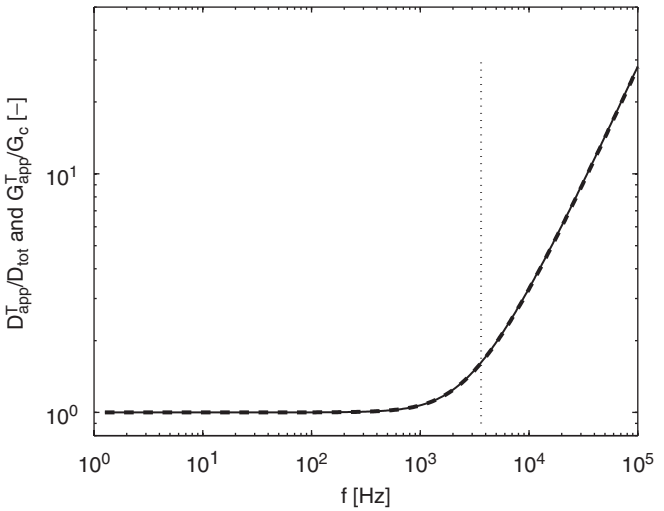

Fig. 9. Equivalent normalized Timoshenko bending stiffness and shear modulus for the sandwich beam specified in Table 3. The dotted line represents $f = f_{\text{mid}}$.

where $D^{\text{T}}_{\text{app}}$ and $G^{\text{T}}_{\text{app}}$ are the apparent bending stiffness and shear modulus. Now, identifying the coefficients of the polynomials yields

$$D^{\text{T}}_{\text{app}}(\omega) = \frac{\mu_{\text{tot}}\omega^2}{\kappa_1^2\kappa_2^2}, \tag{54}$$

$$G^{\text{T}}_{\text{app}}(\omega) = \frac{\mu_{\text{tot}}\omega^2}{h_c(\kappa_1^2 - \kappa_2^2)}. \tag{55}$$

Thus, by calculating κ_1 and κ_2 from Eq. (13) with $I_{\text{tot}} = 0$, we can obtain the equivalent bending stiffness and shear modulus parameters for a Timoshenko beam with arbitrary boundary conditions. As can be seen in Fig. 9, the equivalent shear modulus $G^{\text{T}}_{\text{app}}$ is approximately constant and equal to G_c for low frequencies, while at the high-frequency end of the spectrum it increases rapidly. This is due to the fact that in ordinary Timoshenko theory, the high-frequency asymptote of the main propagating wavenumber denotes a shear wave, not a flexural wave as is the case for the sixth-order sandwich theory. It follows that the dynamic shear modulus will yield an apparent κ_1 wavenumber equal to that of the higher-order theory.

Analogously, the high-frequency asymptote of the nearfield wavenumber is a constant and depends on the ratio of $G^{\text{T}}_{\text{app}}$ to $D^{\text{T}}_{\text{app}}$. Thus, the dynamic bending stiffness $D^{\text{T}}_{\text{app}}$ will display the same high-frequency behaviour as $G^{\text{T}}_{\text{app}}$, see Fig. 9.

The low-frequency asymptote converges towards the static pure bending stiffness D_{tot}.

Asymptotically, the ratio of $G^{\text{T}}_{\text{app}}$ to $D^{\text{T}}_{\text{app}}$ can be shown to be approximately equal to G_c/D_{tot} when $\omega \to 0$ as well as when $\omega \to \infty$. In the mid-frequency range, the ratio depends on the behaviour of κ_1 and κ_2. An approximate explicit expression for the normalized apparent bending stiffness and shear modulus can be given as

$$\frac{D^{\text{T}}_{\text{app}}(\omega)}{D_{\text{tot}}} \approx \frac{G^{\text{T}}_{\text{app}}(\omega)}{G_c} \approx \begin{cases} 1, & \omega \ll \omega_{\text{mid}}, \\ \dfrac{\sqrt{\mu_{\text{tot}}(D_1 + D_2)}}{G_c h_c}\omega, & \omega \gg \omega_{\text{mid}}, \end{cases} \tag{56}$$

where ω_{mid} is a limit frequency defined by the intersection of the asymptotes,

$$\omega_{\text{mid}} = \frac{G_c h_c}{\sqrt{\mu_{\text{tot}}(D_1 + D_2)}}. \tag{57}$$

Eigenfrequencies can be calculated from standard Timoshenko beam formulae using iterative methods, see for example Ref. [15]. The results are shown in Figs. 10 and 11, from which it is clear that the ordinary

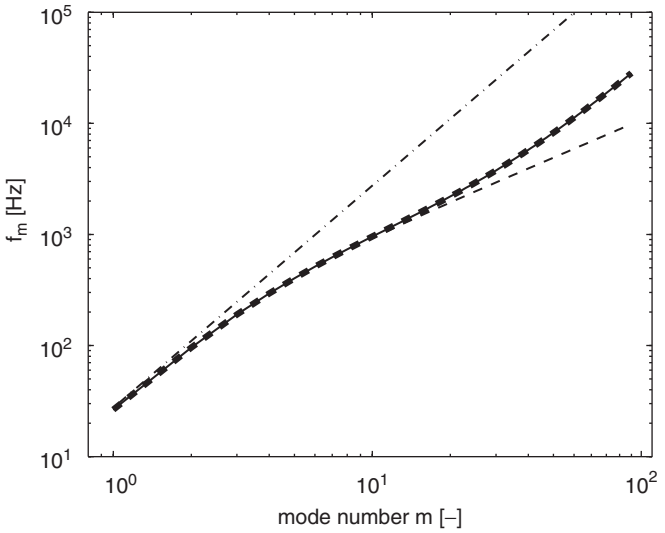

Fig. 10. Eigenfrequencies versus mode number for a simply supported beam—comparison between different models. —, sixth-order model; - -, ordinary Timoshenko theory; - -, modified Timoshenko theory; ···, Bernoulli–Euler theory.

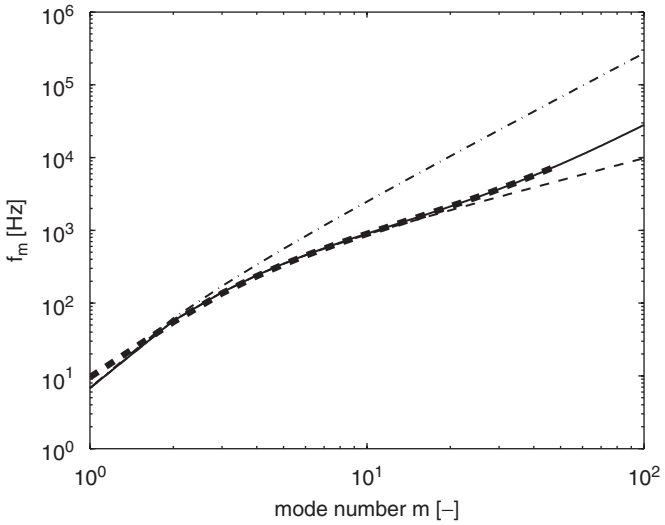

Fig. 11. Eigenfrequencies versus mode number for a clamped–free (cantilever) beam—comparison between different models. —, sixth-order model; - -, ordinary Timoshenko theory; - -, modified Timoshenko theory; ···, Bernoulli–Euler theory.

constant-parameter Timoshenko formula deviates from the value yielded by the higher-order theory, while the agreement between the dynamic parameter model and the higher-order theory is satisfactory over the entire considered range. For the simply supported beam, the resonance frequencies corresponding to the sixth-order theory were obtained from Eq. (21). In the case of the cantilever beam, the resonance frequencies were found by calculating the roots of the determinant Eq. (19). In the latter case, numerical instability occurred above the 48th mode, which is why the curve is truncated.

5. Measurements and validation

In order to validate the models presented in the previous sections, measurements on an asymmetric sandwich beam with both ends free were performed. Material parameters and dimensions are given in Table 3.

Table 3
Approximate material and geometrical properties of the sample sandwich beam used in simulations and measurements

Property	Value
L	1.2 m
h_1	0.75 mm
h_2	2 mm
h_c	10.2 mm
E_1, E_2	70 GPa
E_c	130 MPa
G_c	45 MPa
η_1, η_2	10^{-3}
η_c	4×10^{-2}
ρ_1, ρ_2	2700 kg/m^3
ρ_c	74 kg/m^3

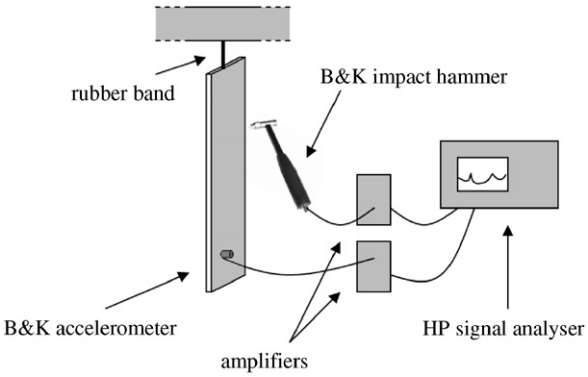

Fig. 12. Measurement setup.

Using an accelerometer and an impact hammer connected to a two-channel signal analyzer, transfer accelerance functions were obtained for a number of different positions of the accelerometer and excitation point. These results were then compared to the predictions of the different models.

In addition, comparisons between the sixth-order model (referred to as "Full model") and the equivalent Bernoulli–Euler model (referred to as "BE-model") were made for simply supported and clamped boundary conditions. For these end conditions, no measured data was obtained due to practical considerations.

5.1. Measurement setup

The measurement setup consisted of a Brüel & Kjær type 4393 accelerometer (weighting 2.4 g) and excitation hammer connected via signal amplifiers to a Hewlett-Packard 3562A signal analyzer, and an asymmetric sandwich beam (see Table 3) suspended in one end by means of an elastic rubber band, imposing approximate free–free boundary conditions (see Fig. 12). The sandwich beam consisted of two aluminum laminates bonded to a plastic foam core. In the HP 3562A analyzer, the 2048-point time record is Fourier transformed into a frequency resolution of 801 lines, from 2 to 1252 Hz with a stepsize of 1.56 Hz. An exponential window was applied to the captured signals. The measurements were performed in the MWL laboratory at KTH, at normal indoor conditions.

5.2. Error sources

The presence of different types of measurement error may influence the validity of the results. For a detailed analysis of this problem, see for example Refs. [16,17]. Some of the possible error sources include the influence

of the added mass of the accelerometer, fluid loading due to surrounding air, low signal-to-noise ratio due to low excitation force impulse or if the accelerometer is close to a node point, possible nonlinear behaviour due to high excitation force impulse and non-ideal boundary conditions. Some of these errors are easily detected; for example, the coherence function—which is obtained for each measurement—will indicate poor quality if the signal-to-noise ratio is low or if nonlinear phenomena are present. The influence of the added mass of the attached accelerometer could potentially be important, especially close to resonance frequencies since the apparent mass of the beam is very low in these regions. It is assumed that the influence of the utilized low-weight accelerometer is negligible in the considered frequency range.

Possible effects of the rubber band supporting the beam are assumed to be negligible. Only free–free boundary conditions were implemented due to the difficulty of achieving other types of configurations, i.e. clamped, simply supported, etc.

5.3. Results

Complex transfer accelerance functions were obtained for a number of different combinations of excitation/reponse coordinates (denoted by x_1 and x_2). The magnitudes of the transfer functions were then plotted together with the predictions yielded by the sixth-order theory and the apparent bending stiffness model. As can be seen in Fig. 13, both models provide reasonably accurate predictions of the transfer accelerance of a free–free sandwich beam, with the exception of the fourth resonance peak. The reason for this behaviour is that either the excitation point or the accelerometer is located close to a node point of the particular mode, and thus the response may change drastically with a small change in position. Indeed, it can be shown that shifting the x_2 coordinate by a few millimeters has great influence on the peak level of the fourth resonance.

The higher-order theory provides near excellent agreement in most of the frequency region considered, while the Bernoulli–Euler theory often fails between the resonances. However, in an acoustic viewpoint this is of no great concern since the resonance peaks contain most of the kinetic energy and thus are of greater importance. The measurement quality is indicated in the coherence plot shown in Fig. 14.

6. Model comparisons

Due to the previously mentioned problems of obtaining results for other than free end conditions during measurements, the special cases of simply supported and clamped conditions were analyzed by comparing the

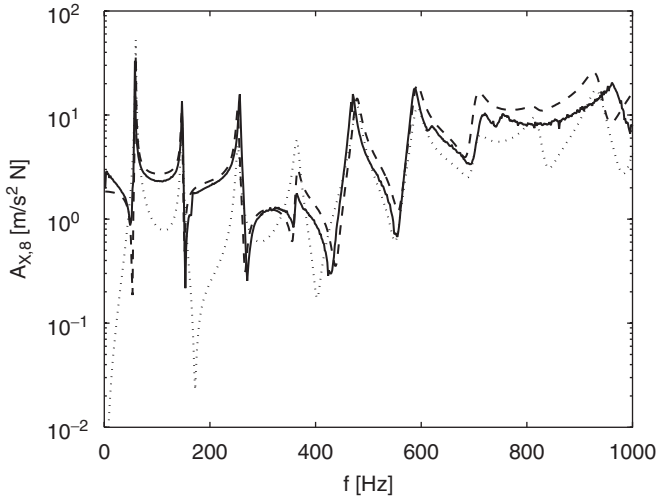

Fig. 13. Transfer accelerance of a free–free beam, $x_1 = 0.19$ m and $x_2 = 0.1$ m. —, measured data; - -, sixth-order model; ···, modified Bernoulli–Euler theory. The fourth peak at around 380 Hz is not well described by either model; this is due to the proximity of the accelerometer or excitation position to a node point for this particular mode.

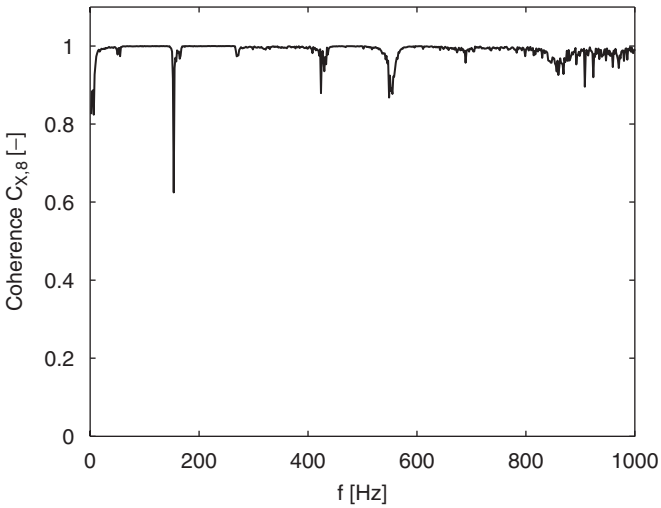

Fig. 14. Coherence of transfer accelerance measurement, $x_1 = 0.19$ and $x_2 = 0.1$ m.

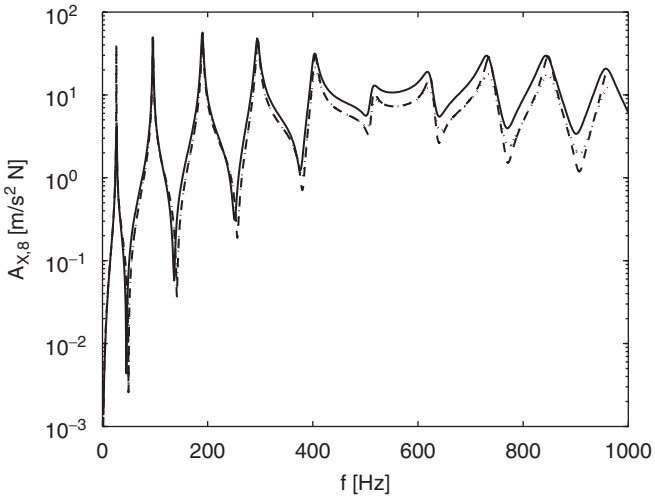

Fig. 15. Predicted transfer accelerance, simply supported ends, $x_1 = 0.19$ m, $x_2 = 0.1$ m. The peak levels in the high-frequency region are better described using the loss factor estimate obtained from Eq. (23). —, sixth-order model; - -, modified Bernoulli–Euler theory, loss factor from Eq. (23); ⋯, modified Bernoulli–Euler theory, loss factor from κ_1.

results of the sixth-order model and the modified Bernoulli–Euler model. As can be seen in the following figures the models agree well, indicating that the simple equivalent Bernoulli–Euler beam theory could be implemented also for these types of boundary conditions.

The loss factor estimate utilized in the calculation of the accelerance of the clamped beam was obtained from the main propagating wavenumber of the higher-order dispersion relation, as described earlier. It could be argued that some other estimate should be used; a lower value of η_{app} in the upper half of the considered frequency region—as indicated in Fig. 8—would improve the agreement of the models. In Fig. 15, curves obtained using the two different estimates of η_{app} are displayed. Note that the peaks of the curve obtained from Eq. (23), using the frequency-dependent bending stiffness $D_{app}(\omega)$, are narrower than those of the higher-order theory—see Fig. 16; this phenomenon can be understood by considering the frequency response of a simple mass–spring system, where the spring "constant" is frequency dependent. By instead using the discrete

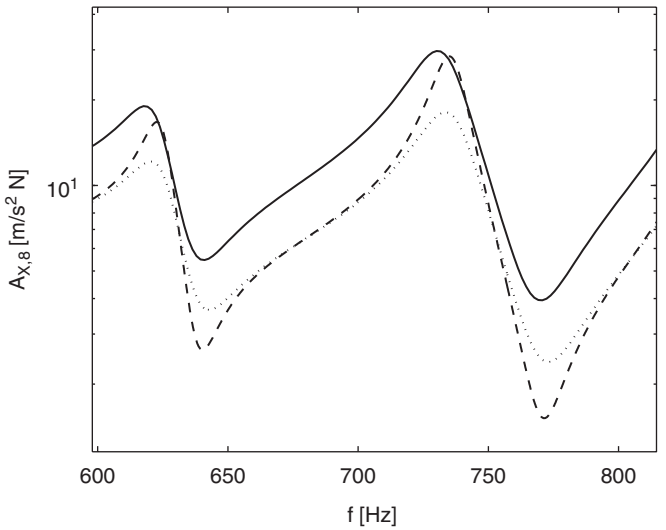

Fig. 16. Detail of Fig. 15, showing the eighth-resonance peak. —, sixth-order model; - -, modified Bernoulli–Euler theory, loss factor from Eq. (23); ⋯, modified Bernoulli–Euler theory, loss factor from κ_1.

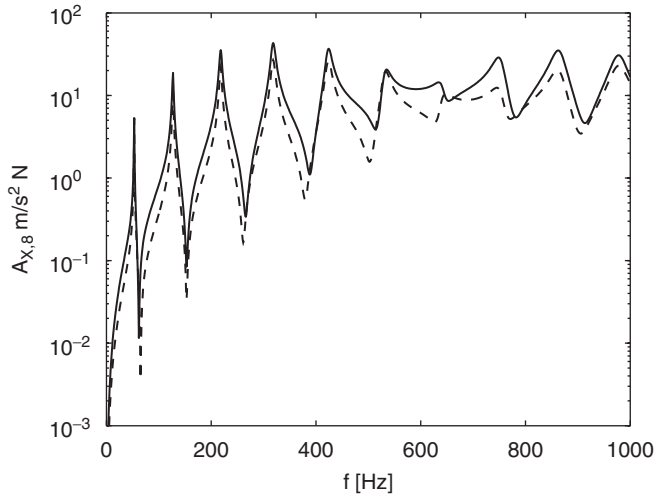

Fig. 17. Predicted transfer accelerance, clamped ends, $x_1 = 0.19\,\mathrm{m}$, $x_2 = 0.1\,\mathrm{m}$. —, sixth-order model; - -, modified Bernoulli–Euler theory.

$D_{\mathrm{app}}^{(m)}$ set of bending stiffnesses—each corresponding to a mode—the problem with narrow peaks is avoided (Fig. 17).

The band-average mobility levels—defined in Eq. (58)—of a simply supported sandwich beam configuration are shown in Fig. 18, indicating again good agreement between the higher-order model and the modified Bernoulli–Euler model. The apparent bending stiffness estimate was obtained from Eq. (23). The band-average mobility levels are given by

$$L_Y^{(m)} = 10\log_{10}\left\{\frac{\dfrac{1}{\omega_{m+1}-\omega_m}\int_{\omega_m}^{\omega_{m+1}} |Y|^2(\omega)\,\mathrm{d}\omega}{Y_{\mathrm{ref}}^2}\right\}, \tag{58}$$

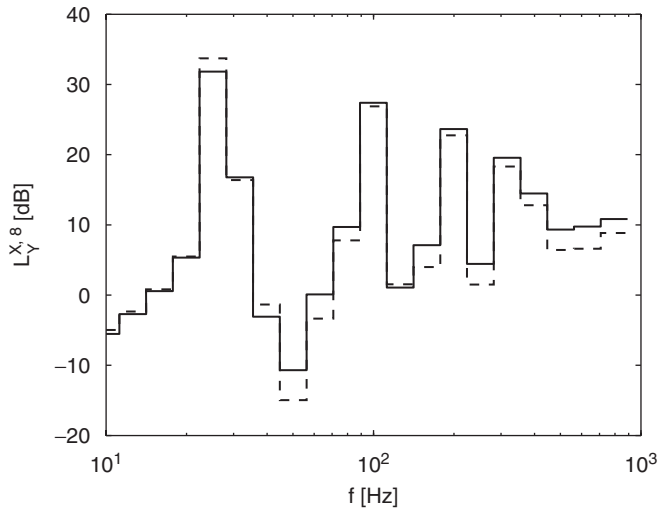

Fig. 18. Predicted mobility levels, simply supported ends, $x_1 = 0.19\,\text{m}$, $x_2 = 0.1\,\text{m}$. —, sixth-order model; - -, modified Bernoulli–Euler method using Eq. (23).

where m is the band number, ω_m is the lower limit frequency of band m and $Y_{\text{ref}} = 10^{-3}$ m/Ns is a reference mobility value.

7. Conclusions

A sixth-order model has been derived which shows excellent agreement with measured data in the frequency range considered. This model, obtained by applying Hamilton's principle, takes into account the shear deformation of the core and the effects of rotational inertia. Obtaining eigenfrequencies, mode shapes and deformations due to external exciting forces using this method implies solving large matrix systems for each frequency line considered. The calculations were performed on a standard PC using the numerical software package Matlab.

In addition, the possibility of using modified lower-order methods—such as the *Bernoulli–Euler* or *Timoshenko* beam theories, in combination with frequency-dependent parameters—to calculate the flexural response of sandwich beams subject to different loading and end conditions has been evaluated. The models have been verified by transfer accelerance measurements on a freely suspended asymmetric sandwich beam with aluminum laminates and a plastic foam core, indicating good agreement.

7.1. Conditions for obtaining satisfactory results using the apparent bending stiffness approach

The following items should be carefully considered in order to obtain satisfactory results using the apparent bending stiffness approach:

- The influence of rotational waves should be considered negligible. This condition is satisfied if $\omega \ll \omega_{\text{rot}}$, where ω_{rot} is defined in Eq. (14).
- The laminates should move in phase, i.e the frequency should be far below the mass–spring–mass frequency of the sandwich beam.
- The laminates should be thin in comparison to the flexural wavelength, so that thin-beam theory is applicable. This condition is satisfied if $h_j\kappa_1 \ll 1$, where $j = 1, 2$ and κ_1 is the wavenumber corresponding to propagating flexural waves.
- In general, there might be problems close to junctions and discontinuities, due to the description of the nearfields.

- As the modes share the same frequency-dependent bending stiffness, the issue of *modal overlap* could arise when consecutive eigenfrequencies become too close. This could be a complicating factor, especially when modelling plates using the apparent bending stiffness technique.
- In order to avoid narrowing of the resonance peaks—and thus an underestimation of the kinetic energy of the structure—the gradient $\mathrm{d}D_{\mathrm{app}}/\mathrm{d}\omega$ of the apparent bending stiffness should be limited.

References

[1] S. Timoshenko, *Schwingungsprobleme der technik*, Verlag von Julius Springer, Berlin, 1932 (in German).
[2] L. Cremer, M. Heckl, *Structure-borne Sound*, Springer, Berlin, Heidelberg, New York, 1973.
[3] A.C. Nilsson, Vibroacoustics, TRITA-FKT 2000:14 and 2000:15, ISSN 1103-470X, ISRN KTH/FKT/N–00/14–SE and ISRN KTH/FKT/N–00/15–SE, Stockholm 2000.
[4] E.M. Kerwin Jr., Damping of flexural waves by a constrained viscoelastic layer, *The Journal of the Acoustical Society of America* 31 (7) (1959) 952–962.
[5] D.J. Mead, S. Markus, The forced vibration of a three-layer, damped sandwich beam with arbitrary boundary conditions, *Journal of Sound and Vibration* 10 (2) (1969) 163–175.
[6] J.W.S. Lord Rayleigh, *The Theory of Sound—Part 1*, 1877. (Reprinted 1945 by Dover Publications, New York, ISBN 0486602923.)
[7] A.C. Nilsson, Wave propagation in and sound transmission through sandwich plates, *Journal of Sound and Vibration* 138 (1) (1990) 73–94.
[8] S.S. Sander, Wave propagation in sandwich structures, TRITA-FKT 2001:01, ISSN 1103-470X, ISRN KTH/FKT/DA-01/01-SE, Stockholm 2001.
[9] S.V. Sorokin, Analysis of wave propagation in sandwich plates with and without heavy fluid loading, *Journal of Sound and Vibration* 271 (2004) 1039–1062.
[10] Y.V.K.S. Rao, B.C. Nakra, Vibrations of unsymmetrical sandwich beams and plates with viscoelastic cores, *Journal of Sound and Vibration* 34 (3) (1974) 309–326.
[11] D.J. Mead, A comparison of some equations for the flexural vibration of damped sandwich beams, *Journal of Sound and Vibration* 83 (3) (1982) 363–377.
[12] E. Nilsson, A.C. Nilsson, Prediction and measurement of some dynamic properties of sandwich structures with honeycomb and foam cores, *Journal of Sound and Vibration* 251 (3) (2002) 409–430.
[13] D. Backström, Modelling the flexural dynamics of sandwich beams using Bernoulli–Euler or Timoshenko theory with frequency dependent parameters, TRITA-AVE 2004:45, ISSN 1651–7660.
[14] E. Nilsson, Some dynamic properties of honeycomb structures, TRITA-FKT 2000:30, ISSN 1103-470X, ISRN KTH/FKT/L–00/30–SE.
[15] D. Zenkert, An introduction to sandwich construction, Engineering Materials Advisory Services Ltd., ISBN 0 947817 77 8.
[16] J.S. Bendat, A.G. Piersol, *Engineering Applications of Correlation and Spectral Analysis*, Wiley, New York, 1980 ISBN 0-471-05887-4.
[17] C.M. Harris (Ed.), *Handbook of Acoustical Measurements and Noise Control*, Acoustical Society of America, Melville, New York, 1998, ISBN 1-56396-774-X.